A new method of nowcasting wildfires and impacts: a case study for the USA

Panayiotis K. VAROTSOS[1,2*] Maria N. EFSTATHIOU[1]

[1]Climate Research Group, Division of Environmental Physics and Meteorology, Faculty of Physics, National and Kapodistrian University of Athens, University Campus Bldg. Phys. V, Athens 15784, Greece

[2]Department of Operational Informatics and Geospatial Analysis, Division of Informatics and Telecommunications, Hellenic Fire Brigade, Athens 18346, Greece

[*]Corresponding author: P.K. Varotsos

Email: panvar@phys.uoa.gr

GRAPHICAL ABSTRACT

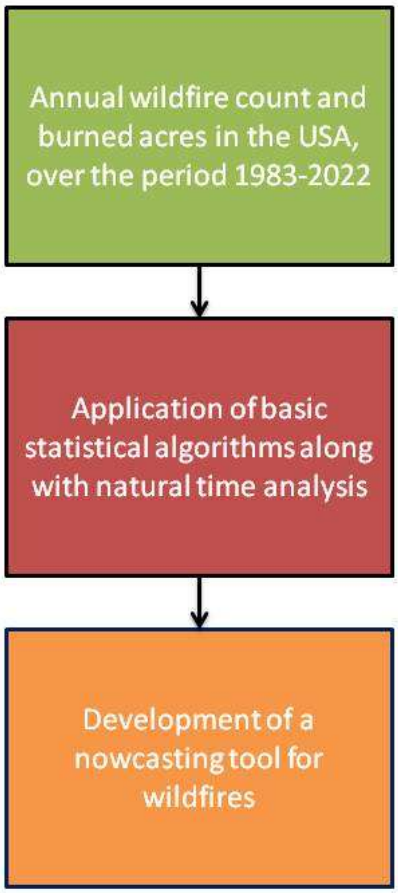

ABSTRACT

In recent years, there has been a steady increase in the intensity and frequency of wildfires worldwide mainly due to the escalating climate crisis and land-use change. Wildfires result in a decline in air quality and cause damage to property, crops, resources, wildlife, and human lives. Since models predict that the number of wildfires will rise by 50% by 2100 the reduction of the wildfire risk is more crucial than ever. We herewith attempt to develop a simple model for nowcasting such catastrophic events that may be useful for preparing authorities and policymakers. As an example, the case of the USA is presented by analyzing the count of wildfires and acres burned there over the past four decades to forecast such catastrophic events over the next ten years. The approach employed in this research can serve as an additional resource in the field of environment and fire ecology, aiding in identifying fire-adapted ecosystems and fire patterns.

Keywords: Environment, fire ecology, nowcasting tool, fire risk

1. Introduction

The wildfires of the last five years in Australia, Canada, the United States, Nepal, the Amazon, Siberia, and Europe have caused heavy loss of lives and property and the destruction of vast acres of land and forests with consequent implications for the success of the Sustainable Development Goals (SDGs) (Dye *et al*., 2023; Pokharel *et al*., 2023). Namely, the recent 2023 Hawaii wildfires have resulted in a tragic loss of a minimum of 96 individuals and incurred a staggering $5.52 billion in damages (Marris, 2023). Prior to the occurrence of the event, a discernible and ascending pattern in the frequency of wildfires within the state of Hawaii had been found (Maui County, 2021). Similarly, the 2021 fire season in Greece, which led to widespread destruction with over 130,000 hectares of burnt area, was one of the most devastating in recent years (Giannaros *et al.*, 2022).

Wildfires are known to be caused by a combination of climatic parameters (e.g., temperature, precipitation, wind, and atmospheric humidity), vegetation, and land use and therefore, in addition to human activities (lighting vegetation fires to clear land for agriculture, grazing, conflicts, etc.),

are governed by the impacts of climate change (Cobb, 2022; Molder and Calice, 2023). Gaining a comprehensive understanding of the environmental impacts of wildfires requires a clear understanding of their dynamics, including factors such as hazards, spatial distribution, and impacts (Szpakowski *et al.*, 2019).

Very recently it was found that towering clouds of smoke rising into the stratosphere from wildfires deplete the ozone layer due to the smoke aerosols, atmospheric chemistry and solar ultraviolet radiation (Solomon et al., 2023, Kondratyev et al., 1994).

Little is known about how environmental and social factors differ between lightning-caused and human-fueled wildfires. Abatzoglou *et al.* (2018) studied differences in temperature, vapour pressure deficit, fuel moisture, and wind speed for large and small lightning- and human-caused wildfires during the first days of fire activity in the USA.

Marlon *et al.* (2012) employed sedimentary charcoal accumulation rates to create long-term fluctuations in fire in the American West over the past 3,000 years. They compared this record with independent fire-history data from historical records and fire scars. They also suggested that burning has decreased over the past 3,000 years, with the lowest levels occurring during the twentieth century and the Little Ice Age.

The onset of a wildfire is influenced by a complex interplay of non-linear dynamics within various environmental components. These components, including vegetation, weather patterns, and topography, exhibit intricate relationships that can lead to rapid and unpredictable shifts in fire behavior (Moritz et al., 2014). For instance, as vegetation accumulates, it becomes more susceptible to ignition, and its moisture content affects its flammability (Pechony & Shindell, 2010). Weather conditions, such as wind speed, humidity, and temperature, interact nonlinearly to create conditions conducive to fire spread. The topography of the landscape influences fire's rate of spread, intensity, and direction, creating localized wind patterns and areas of fuel concentration (Dennison et al., 2014). These non-linear interactions highlight the challenge of predicting wildfire behavior and the need for holistic models that account for the intricate relationships among environmental factors.

Effective wildfire management requires an understanding of these non-linear dynamics to enhance preparedness, response, and mitigation strategies (Parisien et al., 2012; Bowman et al., 2017).

Syifa *et al.* (2020) generated a pre- and post-wildfire map to provide baseline data for evacuation and mitigation planning, in response to the catastrophic wildfire reported in Butte County, California on 08/11/2018, with about 88 deaths and 18,804 structures.

Wildfire risk has increased, but we can still influence where and how wildfires happen. The devastating consequences of the increasing frequency and intensity of wildfires on people's lives and ecosystems require concrete action at all levels, such as developing new integrated management strategies and international cooperation (Lang and Moeini-Meybodi, 2021). The use of the “risk analysis” method in wildfire control has steadily increased over the past ten years. “Risk analysis” is particularly suited to analyzing the timing, location, and potential impacts of wildfires, as it arose out of the need to make decisions about highly unpredictable events. In this regard, Miller and Ager (2012) reviewed recent improvements in estimating and integrating the three components of wildfire risk, "likelihood, intensity, and impacts".

In the studies of risk analysis, the type of the distribution of the used quantities is crucial. Among the most observed data distributions in nature are the Gaussian distribution (or due to its graph "Gaussian bell"), and the semi-logarithmic distribution. In the first case, the majority of the data is gathered into a measure with some dispersion or variance that is symmetric with a fixed mean and variance, thus allowing us to make predictions about an unknown value. In the second case, distribution characterizes the growth of a quantity when it is exponential (Varotsos et al., 2009). A tool to investigate the existence and the properties of the exponential behavior is the rescaled range analysis (Ying et al., 2019). Related to this issue, Efstathiou and Varotsos (2012) showed that the Sahel precipitation anomalies and rainfall index do not follow a Gaussian distribution, but instead, their values seem to obey the semi-logarithmic distribution.

This study attempts to develop a new nowcasting tool for wildfires (NTW) and implement it, using data from the past forty years on the number of wildfires and burned acres in the USA. A

similar methodology has been applied by Varotsos *et al.* (2020), where a novel nowcasting tool for climate parameters was developed.

2. Materials and methods

In an effort to develop a new NTW, we use the annual wildfire count (WFC) and the burned acres (BAC) in the USA, over the period 1983-2022, obtained from the National Interagency Incident Communications Division (NIICD) web page (https://www.nifc.gov/fire-information/statistics). NIICD is a partnership between the United States Department of Agriculture (USDA) Forest Service and the Department of the Interior's agencies. It is located at the National Interagency Fire Center (NIFC) in Boise, Idaho.

The methodology employed to develop the new NTW is the basic statistical algorithms along with the Natural Time Analysis (NTA), which has been introduced by our group at the National and Kapodistrian University of Athens (e.g., Varotsos et al., 2012). The NTA operates on a new perspective of the time platform that determines when a complex system approaches criticality. In short, for a time series of N events, an index to the occurrence of the k-th event is defined by $\chi_k = k/N$, which is called "natural time". In this way, the time intervals between successive events are ignored, but the sequence of events and their energy Q_k are preserved because these two quantities are considered important for the evolution of the system. Next, we study the evolution of the pair (χ_k, Q_k) to forecast upcoming wildfires moving from long-term to short-term scales.

3. Results and Discussion

The first goal of our analysis for implementing NTW development is to identify the most suitable distribution describing WFC and BAC values, to forecast the frequency of such devastating incidents during the next decade.

3.1 The case of WFC

Our investigation begins by plotting the cumulative count (N) of WFC values greater than or equal to M against the values of M itself, covering the period from 1983 to 2022. The Gaussian cumulative distribution function gives an obvious fit to extreme values of WFC (greater than 66481) (Fig. 1a).

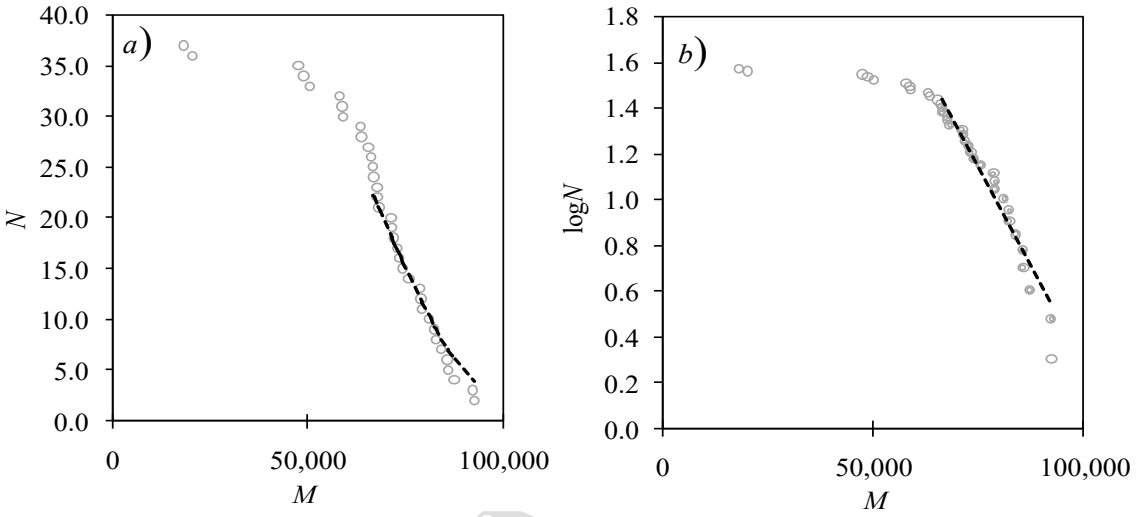

Figure 1. (*a*) Plot of the cumulative frequency-magnitude distribution (gray circles) for WFC over the period 1983-2022, in the USA. The black dashed curve is the fit of the Gaussian cumulative distribution function with $R^2 = 0.97$. (*b*) The semi-logarithmic plot of the cumulative frequency-magnitude distribution (gray circles) for the same WFC dataset. The black dashed line is the GR-scaling least-squares fit, $y = 3.72 - 3.4 \cdot 10^{-5} \cdot x$ and $R^2 = 0.96$.

The *M*–value 66481 is chosen to give the best fit, while, according to the *F*-test, the coefficient of determination $R^2 = 0.97$ is statistically significant at the 95% confidence level.

Furthermore, applying the non-parametric Kolmogorov-Smirnov (KS) test to the above-mentioned values gives a KS-statistic $D = 0.077$ which is below the critical value (at 95% confidence level), confirming that the WFC is normally distributed.

Next, we show in Fig.1b the logarithm of N of WFC values greater than or equal to M versus M (Varotsos et al., 2020b). Regression analysis shows a statistically significant linear relationship between log$N$ and M regarding extreme WFC values (those exceeding 66481):

$$\log N = d - cM. \quad (1)$$

Once again, the value 66481 is chosen to achieve the most accurate linear fit, while the significance of R^2 = 0.96 (with c = 3.4·10^{-5} and d = 3.72) is assessed using an F-test (*t-test*), at the 95% confidence level. As a result, the cumulative frequency distribution of high WFC values also appears to follow the Gutenberg-Richter (GR) law.

Next, we evaluate the accuracy of the aforementioned GR fit by subjecting the mentioned values to the KS test. The KS-statistic D = 0.097 provides evidence of the semi-logarithmic distribution in the case of high WFC values, with a confidence level of 95%.

However, to confirm the GR-fit, we also employ the concept of the "natural time" (Varotsos et al., 2004, 2012), exploring the cumulative number, N_1, of WFC with magnitude $M \geq M_1$ that occurred after an extremely high WFC with $M \geq M_2$ (see Varotsos et al., 2020a,b). The values of M_1 = 66,481 and M_2 = 70,295.87 denote the threshold of the above-mentioned WFC interval and the WFC average during 1983-2022, respectively.

More specifically, we examine whether two values with a fixed difference $d = M_1 - M_2$ exhibit a constant ratio N_2/N_1, as implied by the GR-relation:

$$N_2/N_1 = 10^{c(M_1 - M_2)} = constant \quad (2)$$

where c is calculated from Eq.(1) and N_2 is the cumulative number of FC with size $M \geq M_2$.

Indeed, Fig. 2a presents the pair (N_1, N_2), whenever an extremely high WFC occurs, accompanied by the linear function $F(N_1) = c_0 N_1$ with $c_0 = 10^{c(M_1 - M_2)}$ and an obvious correlation

between these two curves appears, confirming the reliability of the GR-model. The coefficient of determination of this linear fit on the (N_1, N_2) pairs is estimated to be R^2 = 0.99 revealing a prominent significance at the 95% confidence level.

Next, we plot the cumulative number N_1 against the conventional clock time *t* (in years), over the period 1983-2022 and a linear relationship of the type $F(t) = \ell t$ is detected (Fig. 2b). The constant $\ell = 0.65 \pm 0.1$ is calculated by averaging the ratio N_1/t and its confidence interval is $\left(\ell - Z_{\alpha/2}\sqrt{\frac{\ell(1-\ell)}{n}}, \ell + Z_{\alpha/2}\sqrt{\frac{\ell(1-\ell)}{n}}\right)$, where *n* is the count of pairs (N_1, t) and $Z_{\alpha/2}$ is the critical value of the standard normal distribution at *a* significance level.

The coefficient of determination of this linear fit to the pairs (N_1, t) is R^2 = 0.96 indicating high statistical significance at the 95% confidence level.

Fig. 2c clearly shows a strong correlation between observed and nowcasted N_2-values with respect to conventional clock time. The nowcasted N_2-values are estimated using Eq. (2) where we take the N_1-values given in Fig. 2b and multiply them by the slope c_0 (as shown in Fig. 2a). Statistical validation of this agreement is confirmed at the 95% confidence level using the Wilcoxon Signed Rank test.

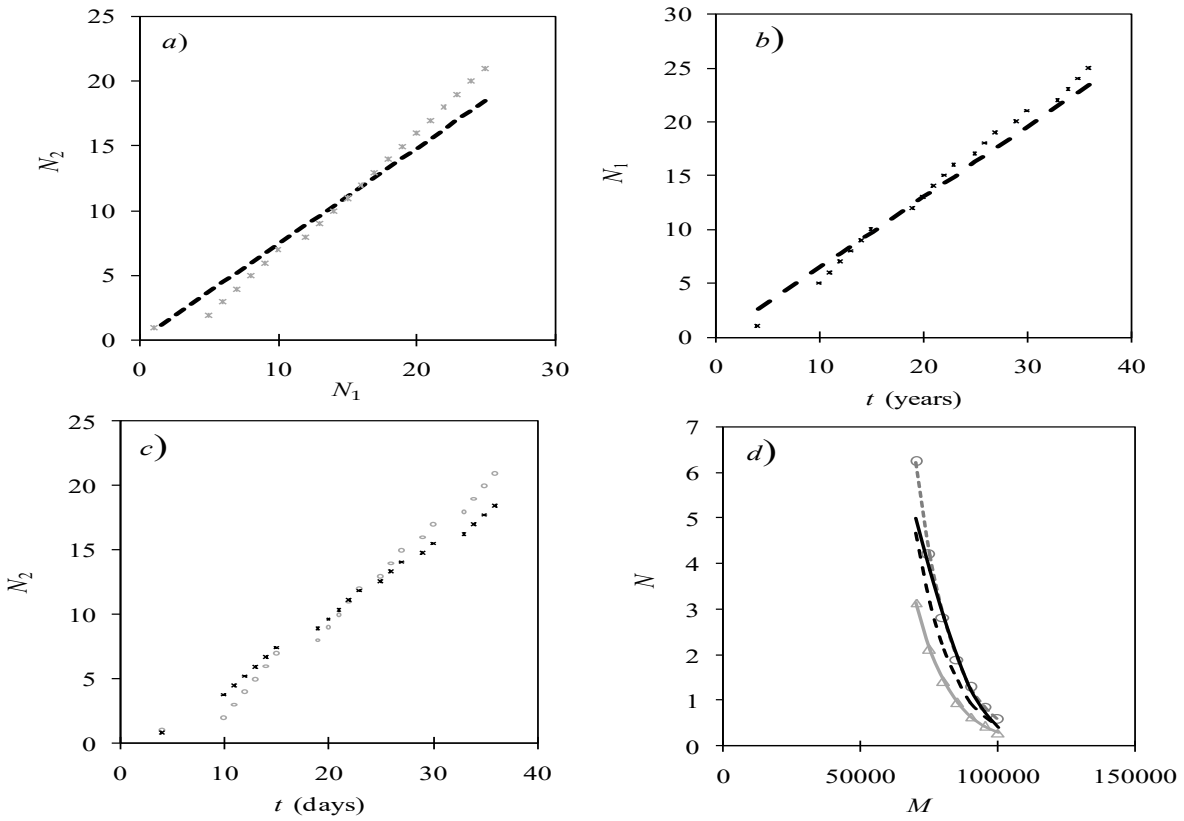

Figure 2. (*a*) Dependence of the cumulative number of extremely high FC, N_2, on the cumulative number of less high values, N_1 (grey points). The dashed black line is the linear fit to the data passing through the origin, with $y = 0{,}74x$ and $R^2 = 0{,}96$. (*b*) Cumulative number, N_1, of WFC with magnitude $M \geq M_1$ vs. the clock time (in years), during 1983-2022, in the USA. The black dashed line is the linear fit to the data, with $y = 0{,}65 \cdot x$ and $R^2 = 0{,}96$. (*c*) Empirical (gray dots) and nowcasted (black dots) N_2- values vs. clock time (in years), for the same period. (*d*) Nowcasted N – values vs. M (for $70{,}296 \leq M \leq 100{,}296$, during 2023-2032) derived from both the Gaussian cumulative distribution function (black solid line) and the "natural time" model (black dashed line) accompanied by the upper (grey dashed line with circles) and lower (grey solid line with triangles) bounds of the 95%-confidence interval of ℓ

Finally, we calculate the nowcasted cumulative number N versus selected magnitudes $70{,}296 \leq M \leq 100{,}296$, for WFC during the next 10 years (i.e., 2023-2032). The nowcasted N is derived from Eq. (2) by replacing N_2 with N, M_2 with the above-mentioned magnitudes, and N_2 with the product of ℓ and the 10-year period:

$$N = 10^{c(M_1 - M)} \cdot 10\,\ell \quad (3)$$

It is worth noting that ℓ seems to remain almost constant for all these magnitudes.

Fig. 2d depicts the nowcasted N versus M (for $70{,}296 \leq M \leq 100{,}296$) derived from both the Gaussian cumulative distribution function and the "natural time" model. The graph also displays the upper and lower limits of the 95%-confidence interval of ℓ.

3.2 The case of BAC

The next step of our analysis is to study the case of BAC. Thus, we investigate the cumulative number (N) of BAC values greater than or equal to M versus M, for the period 1983-2022. The Gaussian cumulative distribution function seems to fit the entire plot significantly. Indeed, according to the F-test, the coefficient of determination $R^2 = 0.95$ is statistically significant at the 95% confidence level (Fig. 3a).

We then apply the KS test to the above-mentioned values and the resulting KS-statistic $D = 0.12$ appears to be lower than the critical value (at 95% confidence level), thus confirming the normal distribution of BAC.

On the other hand, we present the logarithm of N of BAC values greater than or equal to M versus M, accompanied by a linear fit to the entire plot (Fig.3b). The regression analysis gives $R^2 = 0.89$ that is statistically significant at 95% confidence level (according to the F-test). However, the KS test applied to the above-mentioned values gives $D = 0.23$ which is higher than the critical value (at 95% confidence level).

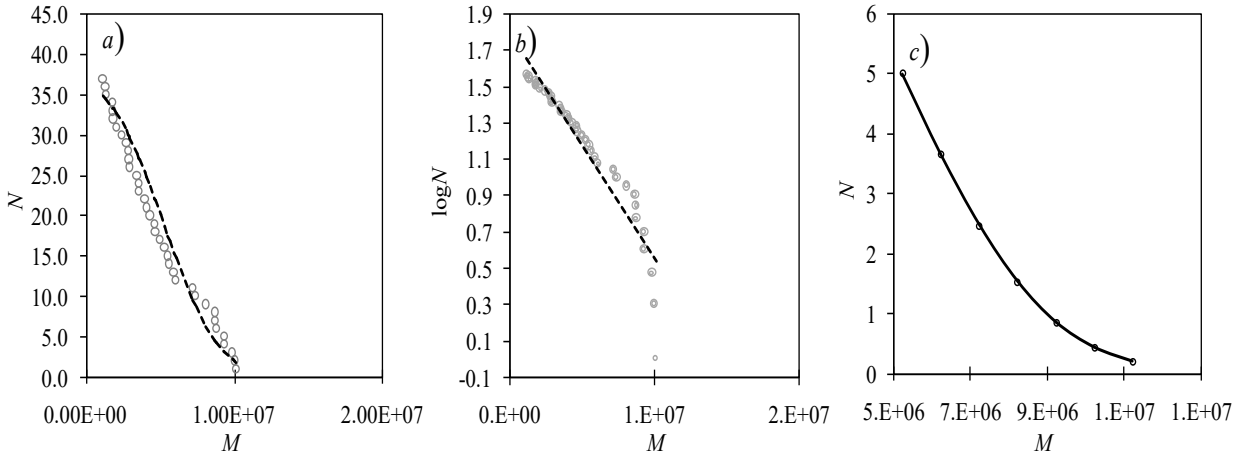

Figure 3. (*a*) Plot of the cumulative frequency-magnitude distribution (gray circles) for BAC during 1983-2022, in the USA. The black dashed curve is the fit of the Gaussian cumulative distribution function with R^2 = 0,97. (*b*) Semi-logarithmic plot of the cumulative frequency-magnitude distribution (gray circles) for the same BAC dataset. The black dashed line is the least-squares fit of the GR-scaling, $y = 1.8 - 1.2 \cdot 10^{-7} x$ and R^2 = 0,89. (*c*) Nowcasted N – values vs. M for the next decade and for $5{,}223.975 \leq M \leq 11{,}223.975$, as derived from the Gaussian cumulative distribution function.

Thus, the BAC values significantly obey only the Gaussian distribution, while the GR-law is not confirmed. Fig. 3 plots the nowcasted N versus M (for $5{,}223.975 \leq M \leq 11{,}223.975$, during 2023-2032) derived from the Gaussian cumulative distribution function.

All the characteristic features found from the analysis above constitute the new simple tool that may be utilized to perform the forecasting and nowcasting of future devastating wildfires in a specific geographic area.

4. Conclusions

In the aforementioned analysis, we proposed a new nowcasting tool for wildfires by investigating the distribution function of both WFC and BAC. As a case study, we presented wildfires that have occurred in the US using available data over the past four decades, with the goal of forecasting and nowcasting such catastrophic events over the next decade. In this effort, the main findings were as follows:

1) The number of large wildfires that occurred in the USA significantly obeys both the Gaussian and the semi-logarithmic distributions. The combination of these two distributions can accurately predict the probability of such devastating events occurring in the next decade, which may contribute to an effective wildfire safety management.
2) The application of "natural time analysis" showed that the GR-law behaviour of the extreme values of wildfire counts is a solid assumption for the proposed nowcasting tool of wildfires.

The proposed above simple nowcasting tool can also contribute insight to management strategies for reducing climate and wildfire vulnerability and increasing habitat sustainability (Folharini et al., 2023). Finally, the model developed in this paper can help support multiple SDG's by enabling more effective management of environmental risks, enchancing disaster resilience, protecting ecosystems and communities, and promoting collaboration and innovation in the pursuit of sustainable development. In particular, the prediction and monitoring of wildfire occurrences, which are influenced by climate factors, can support efforts to mitigate and manage wildfires, thereby addressing one of the key impacts of climate change (Goal 13: Climate action). Also, it can provide valuable information to authorities and communities, enabling them to take proactive measures to prevent wildfires from spreading into populated areas and minimizing damage to infrastructure and homes (Goal 11: Sustainable Cities and Communities).

References

Abatzoglou J.T., Balch J.K., Bradley B.A., Kolden C.A. (2018). Human-related ignitions concurrent with high winds promote large wildfires across the USA, *International Journal of Wildland Fire*, **27**(6), 377-386, https://doi.org/10.1071/WF17149.

Bowman D.M.JS, Williamson G.J., Abatzoglou J.T., Kolden C.A., Cochrane M.A., Smith A.M.S. (2017). Human exposure and sensitivity to globally extreme wildfire events. *Nat. Ecol. Evol.*, **1**(3), 0058.

Cobb, R.C. (2022). The intertwined problems of wildfire, forest disease, and climate change interactions. *Current Forestry Reports*, **8**(2), 214-228.

Cost of Government Commision (2021). Report on Wildfire Prevention and Cost Recovery on Maui. https://www.mauicounty.gov/DocumentCenter/View/129493/Report-on-Wildfire-Prevention--Cost-Recovery-on-Maui---Part-1-Report--Exhibits-A-B-33-MB?bidId=.

Dennison P.E., Brewer S.C., Arnold J.D. and Moritz, M.A. (2014). Large wildfire trends in the western United States, 1984–2011, *Geophys. Res. Lett.*, 41, 2928–2933, doi:10.1002/2014GL059576.

Dye A.W., Gao P., Kim J.B., Lei T., Riley K.L. and Yocom L. (2023). High-resolution wildfire simulations reveal complexity of climate change impacts on projected burn probability for Southern California. *Fire Ecology*, **19**(1), 1-19.

Efstathiou M.N. and Varotsos C.A. (2012). Intrinsic properties of Sahel precipitation anomalies and rainfall, *Theoretical and Applied Climatology*, **109**, 627-633.

Folharini S., Vieira A., Bento-Gonçalves A., Silva S., Marques T., and Novais J. (2023). Bibliometric Analysis on Wildfires and Protected Areas, *Sustainability*, **15**(11), 8536.

Giannaros T.M., Papavasileiou G., Lagouvardos K., Kotroni V., Dafis S., Karagiannidis A. and Dragozi E. (2022). Meteorological Analysis of the 2021 Extreme Wildfires in Greece: Lessons Learned and Implications for Early Warning of the Potential for Pyroconvection. *Atmosphere*, **13**(3), 475, https://doi.org/10.3390/atmos13030475.

Kondratyev K.Ya., Varotsos C.A. and Cracknell A.P. (1994). Total ozone amount trend at St Petersburg as deduced from Nimbus-7 TOMS observations, *International Journal of Remote Sensing*, **15**(13), 2669-2677.

Lang Y. and Moeini-Meybodi H. (2021). Wildfires – a growing concern for sustainable development. UN, Dept. of Economic & Social Affairs, *Future of the World*, Policy brief No 111, 1-4, https://www.un.org/development/desa/dpad/wpcontent/uploads/sites/45/publication/PB_111.pdf.

Marris E. (2023). Hawaii wildfires: did scientists expect Maui to burn? *Nature*, **620**, 708-709, https://doi.org/10.1038/d41586-023-02571-z.

Marlon J.R., Bartlein P.J., Gavin D.G., Long C.J., Anderson R.S., Briles C.E., Brown K.J., Colombaroli D., Hallett D.J., Power M.J., Scharf E.A. and Walsh M.K. (2012). Long-term perspective on wildfires in the western USA, *Proceedings of the National Academy of Science*, **109**(9), E535-E543, https://doi.org/10.1073/pnas.1112839109.

Miller C. and Ager A. (2012). A review of recent advances in risk analysis for wildfire management, *International Journal of Wildland Fire,* **22**(1), 1-14, https://doi.org/10.1071/WF11114.

Molder A.L. and Calice M.N. (2023). What Do Extreme Weather Events Say About Climate Change? Comparing Politicization and Climate Policy in US Wildfire and Hurricane News Coverage. *Environmental Communication,* **17**(4), 370-385.

Moritz M.A., Batllori E., Bradstock R.A., Gill A.M., Handmer J., Hessburg P.F., Leonard J, McCaffrey S., Odion D.C., Schoennagel T. and Syphard A.D. (2014). Learning to coexist with wildfire. *Nature*, **515**(7525), 58-66. doi: 10.1038/nature13946. PMID: 25373675.

Pechony O. and Shindell D.T. (2010). Driving forces of global wildfires over the past millennium and the forthcoming century. *Proc. Nat. Ac. Sci. U.S.A.*, **107**(45), 19167-70, doi: 10.1073/pnas.1003669107.

Pokharel B., Shankar S., Stuivenvolt-Allen J., Wang S.-Y., LaPlante M., Gillies R.G., Khanal S., Wehner M., Rhoades A., Hamal K., Hatchett B., Liu W.-Y., Mukherjee S. and Aryal D. (2023). Amplified drought trends in Nepal increase the potential for Himalayan wildfires, *Climatic Change*, **176**, 17, https://doi.org/10.1007/s10584-023-03495-3.

Solomon S., Stone K., Yu P., Murphy D.M., Kinnison D., Ravishankara A.R. and Wang P. (2023). Chlorine activation and enhanced ozone depletion induced by wildfire aerosol, *Nature*, **615**(7951), 259-264. doi:10.1038/s41586-022-05683-0.

Syifa M., Panahi M. and Lee C.-W. (2020). Mapping of Post-Wildfire Burned Area Using a Hybrid Algorithm and Satellite Data: The Case of the Camp Fire Wildfire in California, USA, *Remote Sensing,* **12**(4), 623, https://doi.org/10.3390/rs12040623.

Szpakowski D.M. and Jensen J.L.R. (2019). A Review of the Applications of Remote Sensing in Fire Ecology. *Remote Sensing*, **11**(22), 2638, https://doi.org/10.3390/rs11222638.

Varotsos C., Efstathiou M., and Tzanis C. (2009). Scaling behaviour of the global tropopause, *Atmospheric Chemistry and Physics*, **9**(2), 677-683.

Varotsos C.A., Mazei Y., Novenko E., Tsyganov A.N., Olchev A., Pampura T., Varotsos C.A., Efstathiou M.N. and Christodoulakis J. (2020a). The lesson learned from the unprecedented ozone hole in the Arctic in 2020; A novel nowcasting tool for such extreme event. *Journal of Atmospheric and Solar-Terrestrial Physics*, **207**, 105330.

Varotsos C., Mazei Y., Novenko E., Tsyganov A.N., Olchev A., Pampura T., Mazei N., Fatynina Y., Saldaev D. and Efstathiou M. (2020), A new climate nowcasting tool based on paleoclimatic data. *Sustainability*, **12**(14), 5546.

Varotsos P.A., Sarlis N.V., Skordas E.S. and Tanaka H. (2004). A plausible explanation of the b-value in the Gutenberg-Richter law from first Principles. *Proceedings of the Japan Academy*, Series B, **80**(9), 429-434, https://doi.org/10.2183/pjab.80.429.

Varotsos P.A., Sarlis N.V. and Skordas E.S. (2012). Order parameter fluctuations in natural time and b-value variation before large earthquakes. *Natural Hazards and Earth System Sciences*, **12**(11), 3473-3481, https://doi.org/10.5194/nhess-12-3473-2012.

Ying H., Shan Y., Zhang H., Yuan T., Rihan W. and Deng G. (2019). The Effect of Snow Depth on Spring Wildfires on the Hulunbuir from 2001–2018 Based on MODIS, *Remote Sens,* **11**(3), 321, https://doi.org/10.3390/rs11030321.